J. Chem. Sci. Vol. 128, No. 2, February 2016, pp. 287–296. © Indian Academy of Sciences.
DOI 10.1007/s12039-015-1022-8

Ab initio adiabatic and quasidiabatic potential energy surfaces of H^+ + CN system

BHARGAVA ANUSURI and SANJAY KUMAR*
Department of Chemistry, Indian Institute of Technology Madras, Chennai 600 036, India
e-mail: sanjay@iitm.ac.in

MS received 15 October 2015; revised 29 November 2015; accepted 3 December 2015

Abstract. We present restricted geometry (collinear and perpendicular approaches of proton) *ab initio* three dimensional potential energy surfaces for H^+ + CN system. The calculations were performed at the internally contracted multi-reference configuration interaction level of theory using Dunning's correlation consistent polarized valence triple zeta basis set. Adiabatic and quasidiabatic surfaces have been computed for the ground and the first excited electronic states. Nonadiabatic effects arising from radial coupling have been analyzed in terms of nonadiabatic coupling matrix elements and coupling potentials.

Keywords. Ion-diatom collisions; *Ab initio* potential energy surface; quasidiabitaziation; Nonadiabatic coupling matrix elements.

1. Introduction

Proton collisions with diatomic target molecules have been studied both theoretically and experimentally over the years. These collisions play an important role in astrophysics and also in molecular physics in understanding the energy transfer mechanism. The choice of proton as projectile is very obvious because it is one of the simplest of ions and collision with it can serve as an archetype for collision studies with bigger ions. Since proton is devoid of any electronic structure, it penetrates the molecular electronic cloud of diatomic molecules upon collision and disrupts it, thereby causing mixing of several electronic states. This leads to nonadiabatic effects arising from the breakdown of the Born-Oppenheimer (BO) approximation.

Cyano radical (CN) is an important constituent in the atmospheres of the Sun, comets, interstellar space and it is also found in hot flames.[1] CN collisional excitation by protons and electrons has been studied to rationalize the cosmic microwave background (CMB) radiation temperature.[2–6]

The bound HCN^+ exhibits the following energy ordering of the low-lying electronic states in the collinear geometry: $X^2\Pi$, $1^2\Sigma^+$, $2^2\Sigma^+$, $1^2\Pi$ and $3^2\Sigma^+$. In the off-collinear geometries, the $^2\Sigma^+$ states correlate with $^2A'$. The $X^2\Pi$ state, which becomes spatially degenerate with the $1^2\Sigma$ state at the collinear geometry, splits into $^2A'$ and $^2A''$ states upon bending as a consequence of symmetry reduction from the $C_{\infty v}$(collinear) point group to the C_s (off-collinear) point group. In the vicinity of the collinear geometry with small off-collinear distortions the potential energy surfaces (PESs) of the non-degenerate states lie very close to each other energetically. Thus, the bound HCN^+ constitutes a Renner-Teller system exhibiting strong vibronic interactions between the ground $X^2\Pi$ state and the first excited $1^2\Sigma^+$ state. The origin of Renner-Teller effect has been explained in different terms in the literature. For a historical account and review, see reference.[7] It arises as a result of, (i) (electrostatic) interaction between the two components of the electronic states with a non-zero angular momentum and, (ii) the electronic-rotational coriolis coupling between the different electronic states. In fact, the Renner-Teller effect arises due to breakdown of the Born-Oppenheimer approximation. Several theoretical developments have been reported on this effect for linear triatomic and tetraatomic molecules. For details, see references[8,9] and references therein. The existence of Renner-Teller coupling complicates the assignments of vibrational progressions. The spectroscopy of HCN^+ poses additional challenge because it can isomerize to HNC^+. Early photoelectron spectroscopy experiments (see reference 6 and references therein) pointed out the difficulties and the challenges in the interpretation of the obtained spectra. High resolution threshold photoelectron spectroscopy[10] recorded eleven rotationally resolved bands and provided information

*For correspondence

on rotational constants, vibronic symmetries and spin-orbit splitting. Latest photoelectron experiments[11] have reported photoelectron spectra of HCN and DCN with further better resolution (less than 4.5 meV or 36 cm^{-1}). Some infrared experimental information is also available for HCN^+ and DCN^+ on a neon matrix.[12]

Early theoretical studies by Köppel *et al.*[13,14] used a model Hamiltonian to treat the vibronic coupling between the $X^2\Pi$ and $1^2\Sigma$ states, which could rationalize the main features observed in the earlier available experimental photoelectron spectra.[15] Subsequent theoretical calculations have been focused on the resolution of the experimentally observed photoelectron spectra. Hansoul *et al.*[16] and Hirst[17] computed the PES for B $^2\Sigma^+(2^2\Sigma^+)$ to ascertain the presence of a local maximum which could explain the appearance of vibrational structure beyond the dissociation limit for this state. Even though the latter obtained the local maximum in the surface, its barrier height was very small to account for the vibrational structure observed. Peterson *et al.*[18] calculated the potential energy surface (pure stretching) of the ground state, $X^2\Pi$ of HCN^+ using single reference configuration interaction (CI) and Dunning's *cc-p*VTZ basis set. They also reported spectroscopic constants obtained by the perturbation theory and bending potential calculated at the equilibrium geometry in the harmonic approximation. Botschwina *et al.*[19] investigated the crossing seam between $^2\Pi$ and $^2\Sigma$ states of HCN^+ using coupled-cluster method. Tarroni *et al.*[20] further extended the theoretical studies and computed *ab initio* adiabatic as well as quasidiabatic potential energy surfaces for the $^2\Pi$ (1 $^2A'$, 1 $^2A''$) and $^2\Sigma^+$ (2 $^2A'$) using internally contracted multireference configuration interaction (*ic*MRCI) to study Renner–Teller and vibronic interactions as a function of internuclear bond distances (r_{CN} and r_{CH}) and angles meaningful for the prediction of experimental spectra. They also studied barrier to isomerization and also computed spin–orbit matrix elements. In view of the availability of high quality photoelectron spectra data[10,11] for the excited $2^2\Sigma^+$ state, and experimental observation of vibrational structure at 22.5 eV, Hirst[21] reported multireference configuration interaction (MRCI) calculations using *cc-p*VQZ basis set obtaining PESs for $X^2\Pi$, $1^2\Sigma^+$, $2^2\Pi$, $2^2\Sigma^+$, $3^2\Sigma^+$, $^4\Pi$ and $^4\Sigma^+$ states. He discussed the photoelectron spectrum of the B $^2\Sigma^+(2^2\Sigma^+)$ in light of the newly computed surfaces and also its pre-dissociation by non-adiabatic transitions.

The present study is focused on constructing global PESs meaningful for the dynamics studies of the H^+ scattering with CN and thereby obtaining information on various excitations and energy transfer processes. The incoming channel, that is H^+ and CN ($X^2\Sigma^+$) with CN in its ground electronic state, correlates to the first excited state ($1^2\Sigma^+$) of the bound HCN^+. Interestingly, the first charge transfer channel, $H(^2S)$ + CN^+ ($X^1\Sigma^+$), which lies just above, and is very close to the entrance channel energetically, correlates with second excited ($2^2\Sigma^+$) state of HCN^+. Therefore, as the first step towards the construction of PESs, we report in the present study the nonadiabaticity arising out of the radial motions of the nuclei, that is, the coupling between the translational motion of H^+ and vibrational modes of CN. Since there is no radial coupling between the $^2\Sigma$ and $^2\Pi$ states, one needs to consider the nonadiabatic interactions between the $^2\Sigma$ states and $^2A'$ states for collinear and off-collinear geometries, respectively. Since the $3^2\Sigma^+$ ($3^2A'$) lies higher in energy, we focus our attention on the $1,2^2\Sigma^+$ and $1,2^2A'$ states. In the present study, we report results for collinear and perpendicular approaches of proton in the scattering (Jacobi) coordinates (see figure 1). The paper is organized as follows: The essential details of the *ab initio* calculations are given in section 2. The characteristics of adiabatic as well as quasidiabatic PESs and their couplings are presented and discussed in section 3, followed by a summary in section 4.

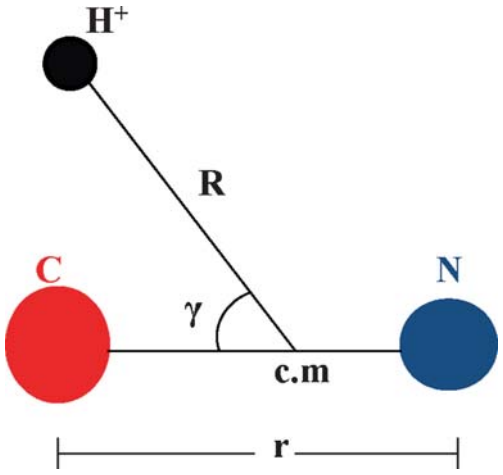

Figure 1. Jacobi coordinates: $\boldsymbol{R}$ is the distance of H^+ from center of mass (c.m.) of CN, **r** is the internuclear distance of CN and $\gamma = \cos^{-1}(\boldsymbol{R}.\boldsymbol{r})$.

2. Theoretical

2.1 *Ab initio calculations*

Adiabatic *ab initio* potential energy surface computations were performed in the Jacobi coordinates (figure 1), where **r** is the interatomic distance of CN, **R** is the

distance of H^+ from the center of mass of CN and $\gamma = \cos^{-1}(\mathbf{R}.\mathbf{r})$ is the angle between **R** and **r**. H^+ approaching C end is considered as 0° and N end as 180°. Calculations were carried out in the C_{2v} symmetry for collinear geometries and in the C_s symmetry for the perpendicular geometry. The ground and the first excited state surfaces were computed for the $^2\Sigma^+$ and the $^2\Pi$ symmetries for the collinear approaches of $H^+$for A′ and A″ states for the perpendicular approach. Computations were done at internally contracted multi-reference configuration interaction[22–24] with Dunning's[25] *cc-p*VTZ basis set using MOLPRO 2010.1[26] suite of programs. At the SCF level, the basis set produced 74 molecular orbitals (MOs) from contracted Gaussian atomic orbitals and they are listed as [33a_1, 17b_1, 17b_2, 7a_2] and [50a′, 24a″] in the C_{2v} and the C_s point groups, respectively. The [1a_1, 2a_1] MOs in the C_{2v} and [1a′, 2a′] MOs in the C_s were treated as core orbitals. The ground state electronic configuration for the $C_{2v}$is [5a_1, 1b_1, 1b_2] with the fifth a_1 orbital singly occupied to give the $^2\Sigma^+$ state and the b_1 orbital singly occupied $^2\Pi$ state accounting for 13 electrons. For the C_s the electronic configuration is [6a′, 1a″] with the sixth a′ orbital singly occupied. In the complete active space self-consistent field (CASSCF)[27,28] calculations, [3-7a_1, 1-2b_1, 1-2b_2] for C_{2v} and [3-9a′, 1-2a″] for the C_s are the active orbitals respectively. The wave function typically consisted of 2308 configuration state functions (CSFs) with 4076 Slater determinants. The configuration interaction (CI) calculations were performed with a reference space of 931 configurations; *N*, *N*-1 and *N*-2 internal configurations were 3139, 2907 and 2304. The total number of contracted configurations was 292058 with 2308 internal, 204296 singly external and 85454 doubly external configurations. The threshold value of the CSFs selection was kept at 3.2×10^{-5} a.u. As a first study, the PES was obtained on the following grid points: $\gamma = 0°$, 90° and 180°; r = 1.4-3.2 (0.1); R = 0.8-1.8 (0.2), 1.9-4.0 (0.1), 4.2-7.0 (0.2), 7.5-10.0 (0.5), 11.0-15.0 (1.0). r and R are in atomic units and the numbers in the parentheses indicate the step size in the interval. Although *a priori* there is no preference for γ in the scattering dynamics, the chosen γ values give a general overview of the topology of the PESs. An example single point energy (in hartrees) for $R = 3.0\ a_o$, $r = 2.23\ a_o$ and $\gamma = 0°$ of $1\ ^2\Sigma^+$ at different levels of theory is listed here: E(SCF) = −92.4126, E(CASSCF) = −92.5789, E(MRCI) = −92.7436 and E(MRCI with Davidson correction) = −92.7510. Since it is well known that Davidson correction is not very reliable at points like avoided crossings, to be consistent throughout we report only energies without Davidson correction in this paper.

3. Results and Discussion

3.1 *Ab initio adiabatic PESs*

We first optimized the equilibrium geometry parameters of the two isomers HCN^+ and HNC^+ and compared them with previously published results in table 1 and table 2. The present results are in good agreement with earlier theoretical results. However, there is a discrepancy regarding r(C-N) in table 1. Interestingly, the present value and the reported values in reference 18 agree well which have been obtained using the *cc-p*VTZ basis set. It is important to point out that calculations in references 17 and 18 were carried out using the *cc-p*VQZ basis set since they required the best possible accuracies in predicting the vibrational progressions of the bound HCN^+ in view of the refined experimental data.[10,11] We carried out calculations with *cc-p*VTZ basis set to obtain the *ab initio* PESs. We believe that they yield sufficient accuracy for scattering calculations since the obtained values of stationary points of the PESs are in close agreement with those obtained earlier with *cc-p*VQZ basis set. For HCN^+ ($\gamma = 0°$), the $1^2\Pi$ state becomes the ground electronic state (GS), that is, lowest in energy, while for HNC^+ ($\gamma = 180°$) the $1^2\Sigma^+$ state becomes the GS. The $1^2\Sigma^+$ is stabler than the $1^2\Pi$ state, and the computed energy difference is found to be 0.979 eV which is in close agreement with that of Tarroni *et al.* (0.996 eV).[17]

Table 1. Optimized geometric parameters of HCN^+ ($A^2\Sigma^+$) bond stretching coordinates, bond angles and their comparison with literature data.

	r(C-H) (a.u)	r(C-N) (a.u)	θ(H-C-N) (degrees)
Present study	2.063	2.309	180
	2.060[a]	2.2982[a]	180[a]
	2.070[b]	2.171[b]	180[b]
	2.060[c]	2.173[c]	180[c]

[a]Reference[18]. [b]Reference[20]. [c]Reference[21].

Table 2. Optimized geometric parameters of HNC^+ ($X^2\Sigma^+$) bond stretching coordinates, bond angles and their comparison with literature data.

	r(N-H) (a.u)	r(C-N) (a.u)	θ(H-N-C) (degrees)
Present study	1.924	2.162	180
	1.921[a]	2.151[a]	180[a]
	1.934[b]	2.162[b]	180[b]

[a]Reference[18]. [b]Reference[20].

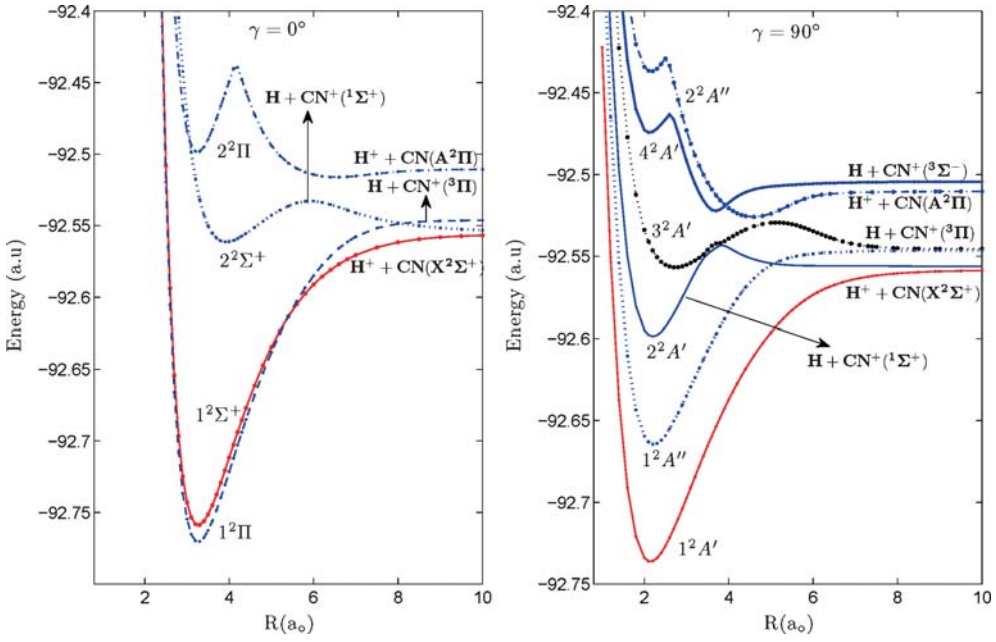

Figure 2. Adiabatic potential energy curves for $\gamma = 0°$ and 90° as a function of R. r fixed at $r_{eq} = 2.23\ a_o$. H is in the ^{2}S state.

We now present in figure 2 the potential energy curves (PECs) as a function of R for r fixed at $r_{eq} = 2.23\ a_o$ for $\gamma = 0°$ and $\gamma = 90°$ for several low lying electronic states. The various asymptotic correlations are also shown. As discussed earlier, the doubly degenerate $^2\Pi$ state in the collinear geometry splits into a ^{2}A′ and a ^{2}A″ states in the off-collinear geometries. The incoming scattering channel corresponds to H^++CN ($X^2\Sigma^+$) correlating with $1^2\Sigma^+$ (collinear) and 1^2A′ (off-collinear) states. Interestingly, the $2^2\Sigma^+$ asymptotically

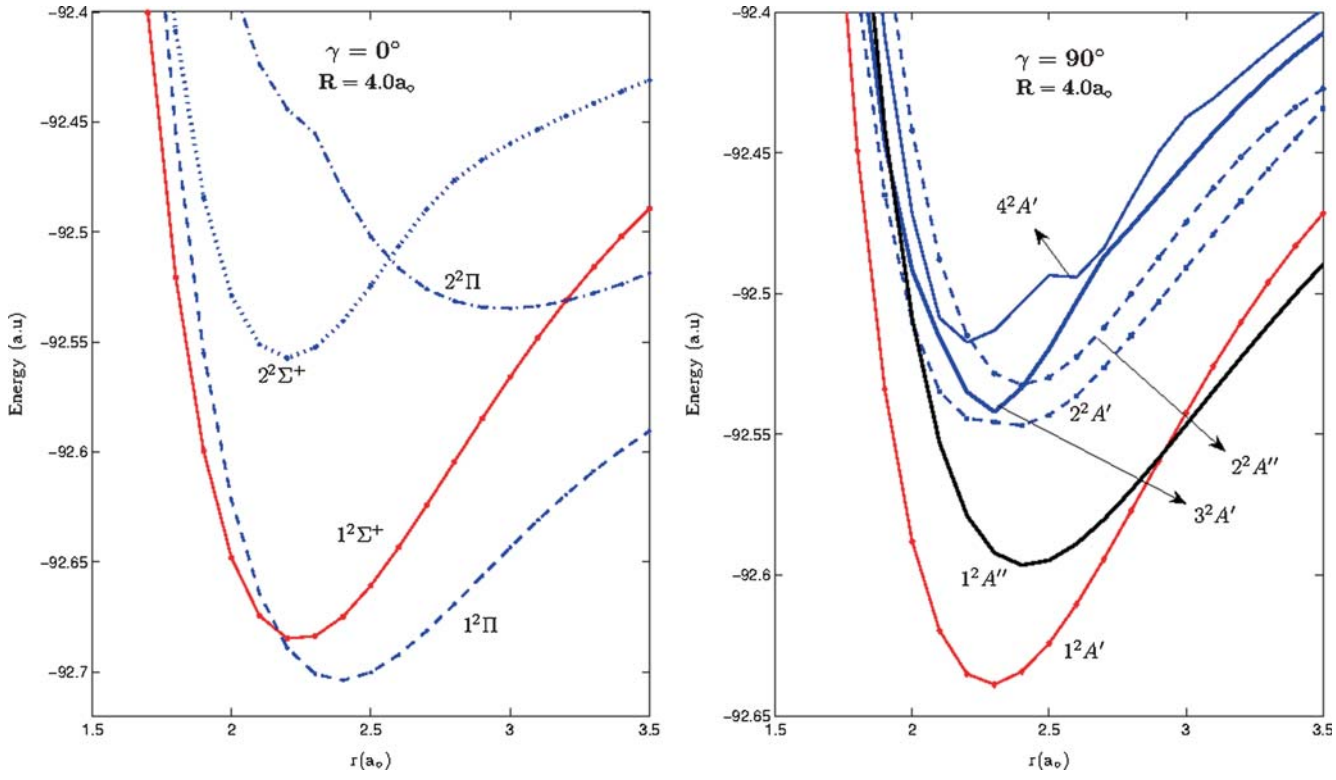

Figure 3. Adiabatic PECs as a function of r for $\gamma = 0°$ and 90° for R fixed at 4.0 a_o.

correlates with the first CT channel, $H(^2S)+CN^+(^1\Sigma^+)$, while the $1^2\Pi$ state correlates with the second CT, $H(^2S)+CN^+(^3\Pi)$. All these asymptotic channels lie close to each other energetically. The endoergicity of the first CT relative to the incoming channel is computed to be 0.278 eV. Similar correlations follow for $\gamma = 90°$. It can be seen that the $1^2\Sigma^+$ and $1^2\Pi$ curves cross at $R = 5.4\ a_o$. In the perpendicular approach each $^2\Pi$ state gives a set of $^2A'$ and $^2A''$ states. One can see that the $2^2A'$, $3^2A'$ and $4^2A'$ states exhibit strong nonadiabatic interactions among themselves in terms of avoided crossings.

As an illustration now we present the PECs as a function of r for a fixed value of $R = 4.0\ a_o$ for $\gamma = 0°$ and $\gamma = 90°$ in figure 3. The Σ and Π PECs cross each other for $\gamma = 0°$. For $\gamma = 90°$, the various $^2A'$ PECs exhibit avoided crossings. The $1^2A''$ and $2^2A''$ appear well-separated energetically and are expected to have less nonadiabatic interactions. In order to have a global view of the nonadiabatic interactions (avoided crossings) the PESs for the lowest two $^2\Sigma^+$ ($\gamma = 0°$ and $\gamma = 180°$) and the $^2A'$ states are shown in figure 4 (left panel) as a function of R and r.

3.2 *Ab initio quasidiabatic PESs*

3.2a *Nonadiabatic coupling matrix elements*: In terms of adiabatic electronic wave functions the coupling between the different electronic states are expressed in terms of the nonadiabatic coupling matrix element (NACME).

$$\left\langle \psi_i^a \left| \frac{\partial^n}{\partial Q^n} \right| \psi_j^a \right\rangle \tag{1}$$

Where $n = 1$ (first-order NACME) or 2 (second-order NACME), and $|\psi_i^a\rangle$ and $|\psi_j^a\rangle$ represent the adiabatic electronic wavefunctions of the involved electronic states (i and j). Q stands for the nuclear coordinates ($\vec{R}$, $\vec{r}$, γ). As mentioned earlier, we are interested in

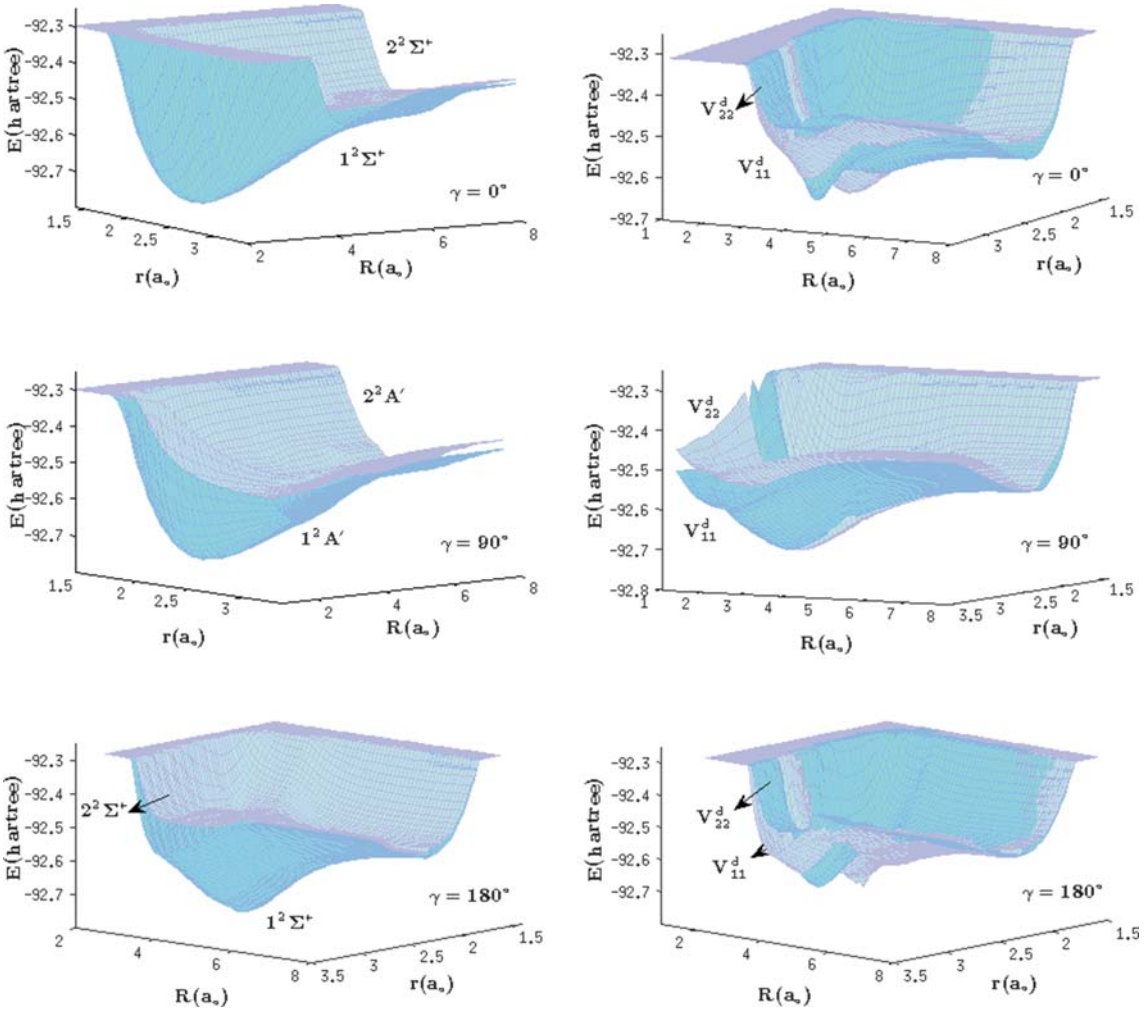

Figure 4. Adiabatic (left panel) and quasidiabatic (right panel) potential energy surfaces as a function of R and r for $\gamma = 0°$, 90° and 180°.

the radial couplings and therefore, here Q stands for $(\vec{R}, \vec{r})$ for a fixed value of γ. The terms with $n = 2$ are generally smaller in magnitude and therefore they are mostly ignored in dynamical calculations.

The first-order NACMEs have been computed between the $1,2^2\Sigma^+$ and the $1,2^2A'$ states by numerical differentiation using the finite difference method.[29]

$$\left\langle \psi_1^a \left| \frac{\partial}{\partial Q} \right| \psi_2^a \right\rangle = \frac{1}{2(\Delta Q)} \left\langle \psi_1^a (Q + \Delta Q) \times \left| \psi_2^a (Q + \Delta Q) \right\rangle \right. \quad (2)$$

Where ΔQ is a small increment. We have used MOLPRO to compute the NACME values using the MRCI wave functions with $\Delta Q = 0.0002\ a_o$. A three dimensional view of NACME as a function of R and r is shown in figure 8. As one can see that in the avoided interaction regions the NACME values exhibit a sharp variation over a small increment of R and r.

In principle, one could carry out dynamical calculations using the adiabatic set of PESs and the NACMEs. However, the latter grow very large in magnitude near the avoided crossings or even become ill-defined at the conical intersections, thus creating instabilities in the numerical integration of dynamical equations. To circumvent the problem, one generally carries out dynamics study in the "(quasi) diabatic" representation of the electronic wave functions wherein they are assumed to be (nearly) independent of the nuclear coordinates. The adiabatic and diabatic wave functions are related with a unitary transformation matrix and the nonadiabatic couplings arise in the kinetic energy part and the potential energy part, respectively. It is important to note here that a set of adiabatic wave functions are always unique and a unique correspondence exists between a set of adiabatic and diabatic wave functions but for a one-dimensional case only, that is, for a diatom having internuclear distance as a variable for Q. For a

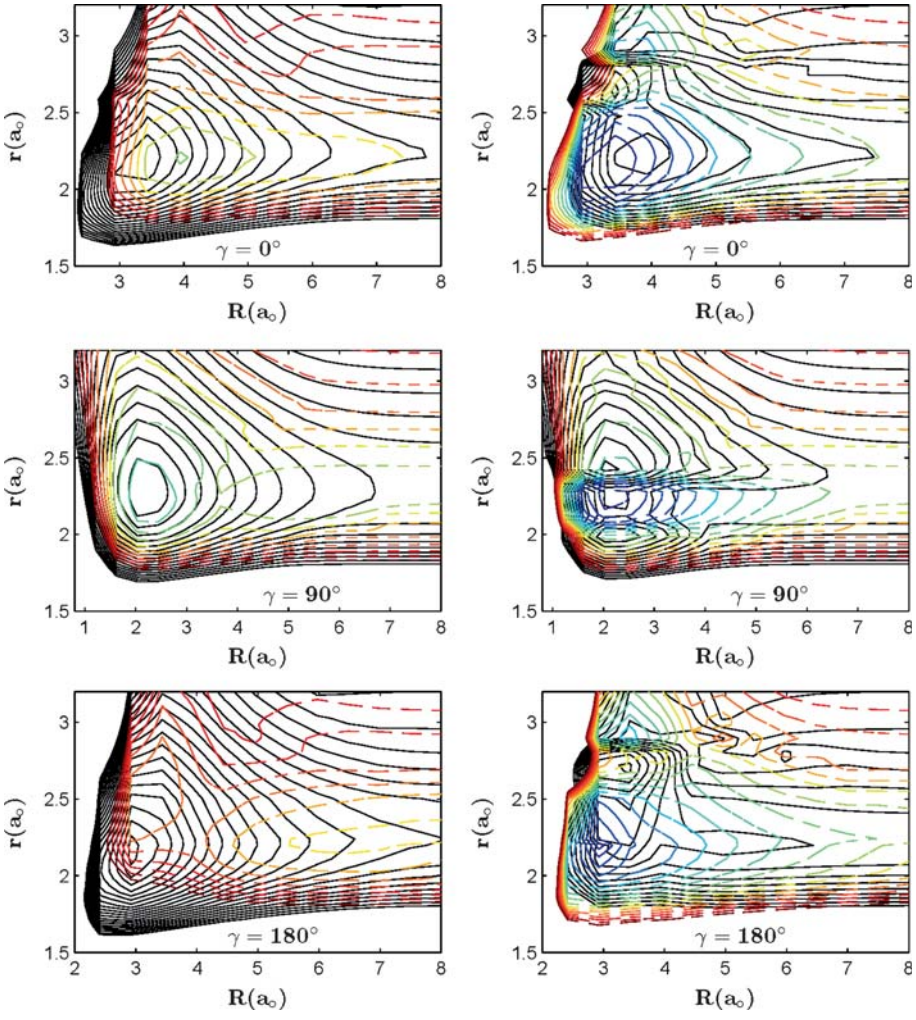

Figure 5. Adiabatic (left panel) and quasidiabatic (right panel) potential energy contours as a function of R and $r$for $\gamma = 0°$, 90° and 180°. Solid lines (–): ground state; broken lines (- -): first excited state.

multi-dimensional case, the transformation between an adiabatic to a diabatic representation is not unique, and therefore different sets of 'quasidiabatic' representations are possible for an adiabatic set, which is always a unique set. This is a serious bottleneck since the dynamics would depend critically on the topologies of quasidiabatic PESs. How to construct a good and reliable set of quasidiabatic PESs have been debated in the literature and many suggestions have been made.[30–46]

It is worth pointing out here that one can obtain the unitary transformation matrix with the prior knowledge of NACME values.[32,33,47] Recently, Adhikari and co-workers[48] studied conical intersections and obtained quasidiabatic PESs for the three lowest electronic states of H_3^+, and carried out time-dependent wave packet dynamics[49] for $D^+ + H_2$ system at low collision energy (T=100 K) using the lowest PES of the system.

In the present study, we have adopted the *ab initio* procedure suggested by Werner and coworkers.[46] In this procedure, the ψ_a's and ψ_d's are assumed to be identical at some Q_{ref} far away from the nonadiabatic interaction region. As one advances slowly towards it, the ψ_a's (and their energies) vary slowly as they are dependent (parametrically) on the nuclear coordinates. The ψ_d's are obtained with the condition that they (and their energies) are nearly independent of Q. This condition is achieved by maximizing the overlap for all pairs of active orbitals at Q_{ref} with those at Q (in the neighborhood of Q_{ref}). One obtains the coupling potential matrix from the transformation matrix between ψ_a's and ψ_d's. This procedure was applied[46] to explain the experimental observation of the photo-dissociation of H_2S by undertaking quantum dynamics on coupled (2x2) electronic PESs. A new set of quasidiabatic potential matrix (2x2) involving the GS and the first excited state $H^+ + H_2$ system was also obtained in our group[50–52] using this procedure and quantum dynamics yielded results in excellent quantitative agreement with those obtained from state-selected experiments. Couplings involving the lowest five ESs (5x5) have also been computed by Balint-Kurti *et al.,* (see General Discussion)[43] using the same procedure.

In the present study, we used Q_{ref} at $R = 16\ a_o$ for both collinear and off-collinear approaches. The obtained quasidiabatic PESs are shown (right panel) along with the adiabatic PESs in figure 4. For better clarity, the same plot is presented as a contour plot in figure 5 to mark the regions of interactions. The adiabatic PESs show avoided crossings. For $\gamma = 0°$ and 180°, we see that quasidiabatic PESs show crossings in different regions which, however is not observed for $\gamma = 90°$. This can be seen better in terms of PECs for adiabatic and quasidiabatic states in figure 6. The quasidiabatic PECs do show crossings in different regions of R for $\gamma = 0°$ and 180°. For $\gamma = 90°$ the quasidiabatic PECs mostly run parallel to the corresponding adiabatic PECs. They however do show crossing (around R = 6.5 a_o) far away from the interaction well. If we analyze the strength of the computed coupling potential (V_{12}) between these two states, we observe that the magnitudes of V_{12} for $\gamma = 90°$ is relatively smaller as compared to those obtained for $\gamma = 0°$ and $\gamma = 180°$. To illustrate it, we have plotted V_{12} as a function of R and r for $\gamma = 90°$ and 180° in figure 7. It is worth noting here that if the coupling potential strengths are relatively smaller then the respective quasidiabatic PECs/PESs may not show crossing in those regions. This behavior has been observed earlier in analysis of model potential coupling[39] and for the H^++ CO system.[53] For an illustration, it would be worthwhile to examine the NACME values for $\gamma = 90°$ which have been plotted as function of R and r in figure 8. NACME shows sharp variations

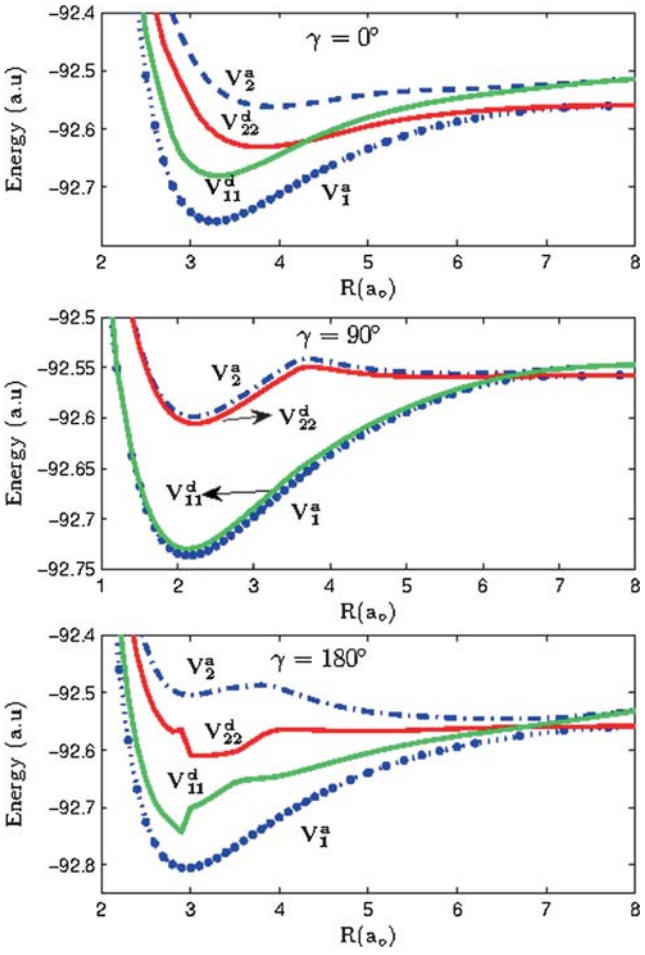

Figure 6. Adiabatic and diabatic PECs for $\gamma = 0°$, 90° and 180°. (V_1^a, V_2^a: $1^2\Sigma^+$, $2^2\Sigma^+$ (for $\gamma = 0°$ and 180°) and $1^2A'$, $2^2A'$ (for $\gamma = 90°$). The corresponding quasidiabatic PECs are designated as V_{11}^d, V_{22}^d, respectively, which are the diagonal elements of the 2x2 coupling potential matrix).

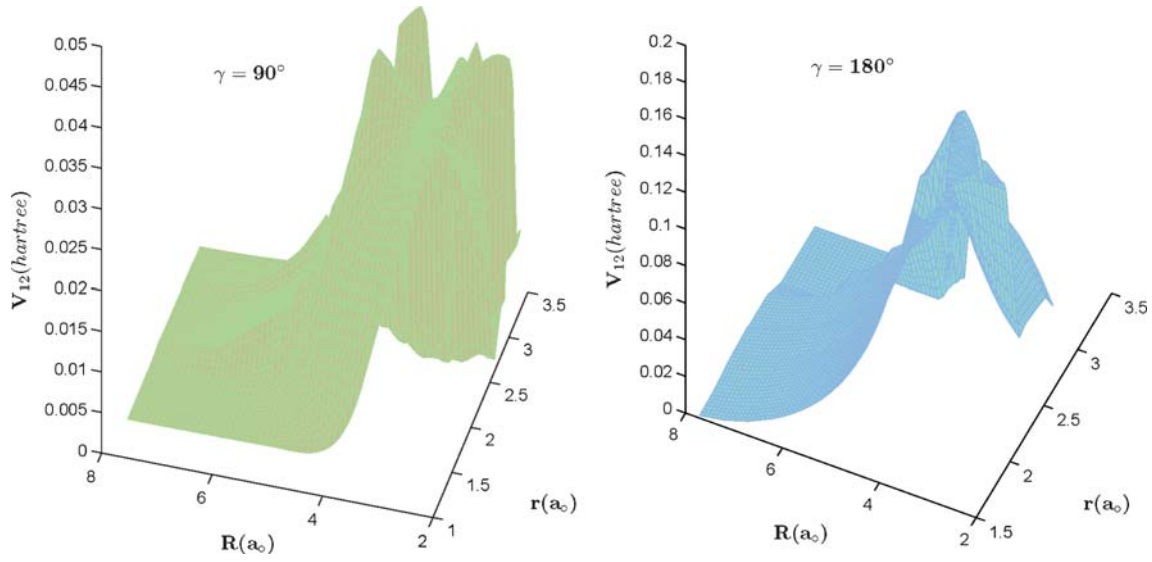

Figure 7. Coupling potentials (V_{12}) between the $1^2\Sigma^+(1^2A')$ and $2^2\Sigma^+$ $(2^2A')$ states as a function of R and r for $\gamma = 90°$ and 180.

around r = r_{eq} = 2.23 a_o and shows its strength even for r less than r_{eq}, and up to R = 8 a_o. One can see in figure 2 ($\gamma = 90°$, right panel) that the $1^2A'$ and $2^2A'$ states come very close energetically around R = 6 a_o and beyond which the PECs for both states run almost parallel exhibiting a Demkov-type of coupling. Note that $1^2A'$ and $1^2A''$ will have no radial coupling. For smaller R, although the two PECs appear to be well separated energetically (see figure 2, right panel), they interact with each other via the Landau-Zener coupling. The Demkov coupling and the Landau-Zener coupling derive their names with the earliest modeling of nonadiabatic interactions involving the two electronic states in two regions. For a general review see reference 53 and references therein. This explains the strength of NACME values for wide range of R as shown in figure 8 around r = r_{eq}. It is also important to note that there is a marked hump in the PEC for the second ES for $\gamma = 90°$

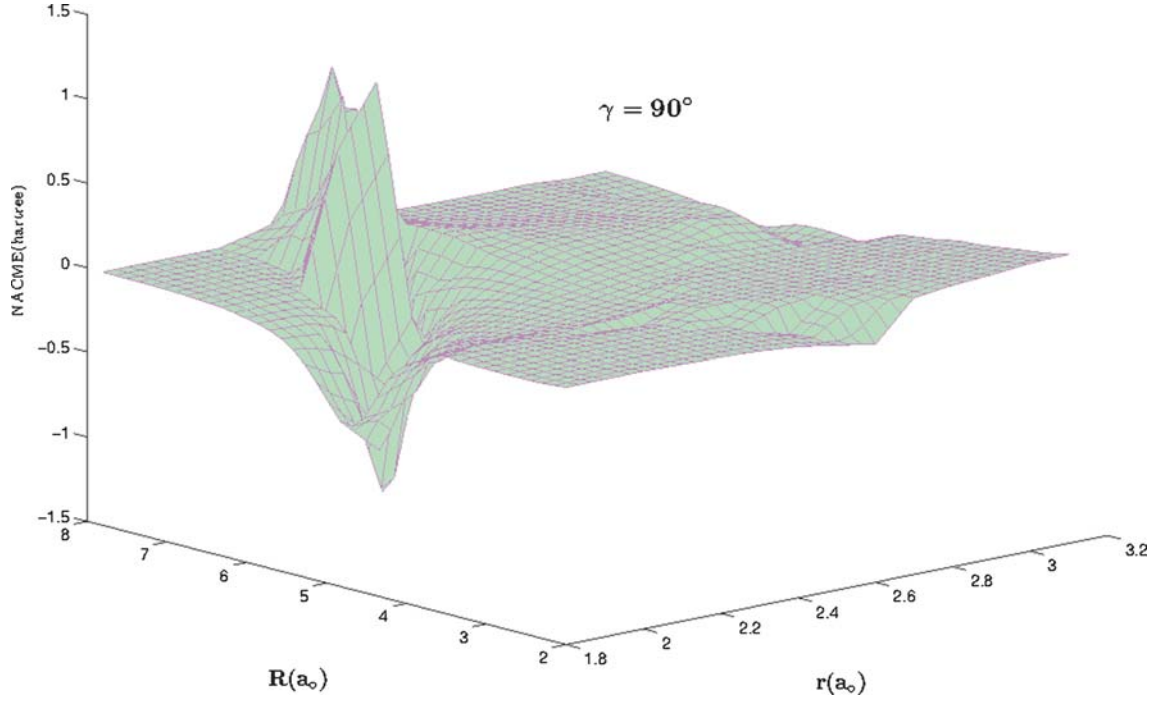

Figure 8. Nonadiabatic coupling matrix elements (NACMEs) involving $1^2A'$ and $2^2A'$ as a function of R and r for $\gamma = 90°$.

(middle inset, figure 6) which is indicative of nonadiabatic interaction of the third ES ($3^2A'$). See also figure 2, right panel. The somewhat irregular behavior of the coupling potential (V_{12}) in figure 7 ($\gamma = 90°$) also reflects this fact. In fact the nonadiabatic interactions get richer with further involvement of the fourth ES ($4^2A'$, figure 2, right panel) for $\gamma = 90°$. Nevertheless, as noted above, the nonadiabatic couplings for the collinear geometry appears to be two to four times higher than that obtained for $\gamma = 90°$ (figure 7). This implies that near-collinear geometry collisions would exhibit higher order of nonadiabaticity at low energies. It would be desirable to compute the global *ab initio* PESs and couplings for other angles which is being undertaken.

4. Conclusions

We have computed adiabatic potential energy surfaces for the ground ($1^2\Sigma^+$ ($1^2A'$)) and the first excited states ($2^2\Sigma^+$($2^2A'$)) of the H^++ CN system. More than 3200 *ab initio* points have been computed for angles $\gamma = 0°$, 90° and 180° at MRCI/*cc-p*VTZ level of theory. The adiabatic curves have avoided crossings which upon diabatization became direct curve crossings. The computed nonadiabatic coupling matrix elements computed show significant interactions between the ground and first excited state. An analysis of the potential coupling indicates that nonadiabaticty between the two states is dominated by near-collinear geometry collisions at low energy. However, the participation of other low-lying ESs would also become possible for moderate collision energies.

Acknowledgements

B.A. thanks IIT Madras and University Grants Commission, New Delhi for providing a research fellowship. High Performance Computing Facility (HPCE) at IIT Madras is also gratefully acknowledged.

References

1. Gaydon A G 1957 In *The Spectroscopy of Flames* (New York: John Wiley)
2. Thaddeus P 1972 *Annu. Rev. Astro. Astrophys.* **10** 305
3. Roth K C and Meyer D M 1993 *Astrophys. J.* **413** L67
4. Leach S 2012 *Mon. Not. R. Astron. Soc.* **421** 1325
5. Allison A C and Dalgarno A 1971 *Astron. Astrophys.* **13** 331
6. Harrison S and Tennyson J 2012 *J. Phys. B: At. Mol. Opt. Phys.* **45** 035204
7. Perić M and Peyerimhoff S D 2002 *Adv. Chem. Phys.* **124** 589
8. Carter S, Handy N C, Puzzarini C, Tarroni R and Palmieri P 2000 *Mol. Phys.* **98** 1697
9. Das A, Mukhopadhyay D, Adhikari S and Baer M 2010 *J. Chem. Phys.* **133** 084107
10. Wiedmann R T and White M G 1995 *J. Chem. Phys.* **102** 5141
11. Eland J H D, Field T, Baltzer P and Hirst D M 1998 *Chem. Phys.* **229** 149
12. Forney D, Thompson W E and Jacox M E 1992 *J. Chem. Phys.* **97** 1664
13. Köppel H, Cederbaum L S, Domcke W and Von Niessen W 1979 *Chem. Phys.* **37** 303
14. Köppel H and Domcke W Cederbaum L S 1979 *Adv. Chem. Phys.* **57** 59
15. Fridh C and Åsbrink L 1975 *J. Electron. Spectrosc. Relat. Phenom.* **7** 119
16. Hansoul J P, Galloy C and Lorquet J C 1977 *J. Chem. Phys.* **68** 4105
17. Hirst D M 1979 *Mol. Phys.* **6** 2017
18. Peterson K A, Mayrhofer R C and Woods R C 1990 *J. Chem. Phys.* **93** 4946
19. Botschwina P, Horn M, Matuschewski M, Schick E and Sebald P 1997 *J. Mol. Struc. (Theochem)* **400** 119
20. Tarroni R, Mitrushenkov A, Palmieri P and Carter S 2001 *J. Chem. Phys.* **115** 11200
21. Hirst D M 2005 *Phys. Chem. Chem. Phys.* **7** 1136
22. Werner H -J and Knowles P J 1988 *J. Chem. Phys.* **89** 5803
23. Knowles P J and Werner H -J 1988 *Chem. Phys. Lett.* **145** 514
24. Knowles P J and Werner H -J 1992 *Theor. Chim. Acta* **84** 95
25. Dunning T H 1989 *J. Chem. Phys.* **90** 1007
26. MOLPRO, version 2010.1, a package of *ab initio* programs, Werner H -J, Knowles P J, Knizia G, Manby F R, Schütz M, Celani P, Korona T, Lindh R, Mitrushenkov A, Rauhut G, Shamasundar K R, Adler T B, Amos D, Bernhardsson A, Berning A, Cooper D L, Deegan M J O, Dobbyn A J, Eckert F, Goll E, Hampel C, Hesselmann A, Hetzer G, Hrenar T, Jansen G, Köppl C, Liu Y, Lloyd A W, Mata R A, May A J, McNicholas S J, Meyer W, Mura M E, Nicklass A, O'Neill D P, Palmieri P, Peng D, Pflüger K, Pitzer R, Reiher M, Shiozaki T, Stoll H, Stone A J, Tarroni R, Thorsteinsson T, and Wang M, see http://wwww.molpro.net
27. Werner H-J and Knowles P J 1985 *J. Chem. Phys.* **82** 5053
28. Knowles P J and Werner H -J 1985 *Chem. Phys. Lett.* **115** 259
29. (a) Werner H –J, Follmeg B and Alexander M H 1988 *J. Chem. Phys.* **89** 3139; (b) Werner H –J, Follmeg B, Alexander M H and Lemoine P 1989 *Chem. Phys.* **91** 5425
30. Smith F T 1969 *Phys. Rev.* **179** 111
31. Mead A C and Truhlar D G 1982 *J. Chem. Phys.* **77** 6090
32. Sidis V 1992 *Adv. Chem. Phys.* **82** 73
33. Pacher T, Cederbaum L S and Köppel H 1993 *Adv. Chem. Phys.* **84** 293
34. Adhikari S and Billing G D 2002 *Adv. Chem. Phys.* **124** 143
35. Baer M 2002 *Adv. Chem. Phys.* **124** 39
36. Baer M 2002 *Phys. Rep.* **358** 75
37. Child M S 2002 *Adv. Chem. Phys.* **124** 1

38. Worth G A and Robb M A 2002 *Adv. Chem. Phys.* **124** 355
39. Jasper A W, Zhu C, Nagia S and Truhlar D G 2004 *Faraday Discuss* **127** 1
40. Köppel H 2004 *Faraday Discuss* **127** 35
41. Vertesi T, Bene E, Vibok A, Halasz G J and Baer M 2005 *J. Phys. Chem. A* **109** 3476
42. Nakamura H 2002 In *Nonadiabatic Transitions: Concepts, Basic Theories and Applications* (Singapore: World Scientific)
43. *General discussion* 2004 *Faraday Discuss.* **127** 81
44. Werner H –J and Meyer W 1981 *J. Chem. Phys.* **74** 5802
45. Heumann B and Schinke R 1994 *J. Chem. Phys.* **101** 7488
46. Simah D, Hartke B and Werner H –J 1999 *J. Chem. Phys.* **111** 4523
47. Sarkar B and Adhikari S 2006 *J. Chem. Phys.* **124** 074101
48. Mukherjee S, Mukhopadhyay D and Adhikari S 2014 *J. Chem. Phys.* **141** 204306
49. Sahoo T, Ghosh S, Adhikari S, Sharma R and Varandas A J C 2015 *J. Chem. Phys.* **142** 124304
50. Saieswari A and Kumar S 2007 *J. Chem. Phys.* **127** 214304
51. Saieswari A and Kumar S 2007 *Chem. Phys. Lett.* **449** 358
52. Saieswari A and Kumar S 2008 *J. Chem. Phys.* **128** 064301
53. George F D X and Kumar S 2010 *Chem. Phys.* **211** 373